JASS Journal of Astronomy and Space Sciences

Characteristics and Geoeffectiveness of Small-scale Magnetic Flux Ropes in the Solar Wind

Myeong Joon Kim[1], Kyung Sun Park[1], Dae-Young Lee[1†], Cheong-Rim Choi[1], Rok Soon Kim[2, 3], Kyungsuk Cho[2, 3], Kyu-Cheol Choi[4], Jaehun Kim[5]

[1]Department of Astronomy and Space Science, Chungbuk National University, Cheongju 28644, Korea
[2]Korea Astronomy and Space Science Institute, Daejeon 34055, Korea
[3]University of Science and Technology, Daejeon 34113, Korea
[4]SELab, Inc., Seoul 06049, Korea
[5]The Korean Space Weather Center of National Radio Research Agency, Jeju 63025, Korea

Magnetic flux ropes, often observed during intervals of interplanetary coronal mass ejections, have long been recognized to be critical in space weather. In this work, we focus on magnetic flux rope structure but on a much smaller scale, and not necessarily related to interplanetary coronal mass ejections. Using near-Earth solar wind advanced composition explorer (ACE) observations from 1998 to 2016, we identified a total of 309 small-scale magnetic flux ropes (SMFRs). We compared the characteristics of identified SMFR events with those of normal magnetic cloud (MC) events available from the existing literature. First, most of the MCs and SMFRs have similar values of accompanying solar wind speed and proton densities. However, the average magnetic field intensity of SMFRs is weaker (~7.4 nT) than that of MCs (~10.6 nT). Also, the average duration time and expansion speed of SMFRs are ~2.5 hr and 2.6 km/s, respectively, both of which are smaller by a factor of ~10 than those of MCs. In addition, we examined the geoeffectiveness of SMFR events by checking their correlation with magnetic storms and substorms. Based on the criteria Sym-H < -50 nT (for identification of storm occurrence) and AL < -200 nT (for identification of substorm occurrence), we found that for 88 SMFR events (corresponding to 28.5 % of the total SMFR events), substorms occurred after the impact of SMFRs, implying a possible triggering of substorms by SMFRs. In contrast, we found only two SMFRs that triggered storms. We emphasize that, based on a much larger database than used in previous studies, all these previously known features are now firmly confirmed by the current work. Accordingly, the results emphasize the significance of SMFRs from the viewpoint of possible triggering of substorms.

Keywords: magnetic flux rope, magnetic cloud, solar wind

1. INTRODUCTION

The interplanetary coronal mass ejection (ICME) is the ejection of a massive amount of material from the Sun's atmosphere, which propagates through interplanetary space. It is often accompanied by a special magnetic field structure called a magnetic flux rope (MFR), also known as a magnetic cloud (MC). When MCs are observed near the Earth, they are characterized by the following key features: (1) smooth rotation of the magnetic field vectors,

(2) stronger magnetic field strength than the ambient interplanetary magnetic field, and (3) lower temperature than the surrounding solar wind (Gosling et al. 1973; Richardson & Cane 1995).

The significance of geomagnetic disturbances caused by ICMEs have long been recognized since ICMEs often carry a strong southward interplanetary magnetic field (IMF) B_z component, which is critical for causing severe space weather near the Earth (Zhang & Burlaga 1988; Gosling et al. 1991; Tsurutani & Gonzalez 1997; Zhang et al. 2007; Richardson

& Cane 2010; Park et al. 2015). Specifically, the ICME is now well-known as the main driver of geomagnetic storms. In addition, many authors have studied storms caused by MCs. For example, Gopalswamy et al. (2015) examined the geoeffectiveness of MCs during solar cycles 23 and 24, and Wu et al. (2016) investigated a strong geomagnetic storm that occurred on March 17, 2015.

Moldwin et al. (1995, 2000) reported the identification of a number of MFR events that were on a much smaller scale compared to normal MFR events. This was named small-scale magnetic flux rope (SMFR). Following this discovery, a limited number of studies regarding SMFRs have been conducted (Feng et al. 2008; Cartwright & Moldwin 2008, 2010), but the basic nature of SMFRs such as occurrence rate, field and plasma structures, and geoeffectiveness still needs to be clarified based on a larger database. More importantly, it remains unclear whether they originate as a structure ejected from solar ejections or due to processes such as magnetic reconnection within the solar wind. Clearly, in these previous studies, SMFRs are considered to be simply a smaller-sized flux rope than MCs. However, it is unclear quantitatively how small they are supposed to be. There is no known boundary in size between SMFRs and MCs. One may even define a kind of intermediate-sized flux rope, namely something between SMFRs and MCs, but again there is no firm way to distinguish among all these definitions of flux ropes of different sizes.

In this paper, we were motivated by the previous studies mentioned above to study SMFRs and see if the previously reported main features of SMFRs remain valid by using a large number of events from a much longer period of 19 years, from 1998 to 2016. Based on the identified events, we determined their main characteristics and compare results with normal MCs. We also examined the geoeffectiveness of SMFRs in terms of storms and substorms, based on Sym-H and AL indices.

2. METHODOLOGY

In this study, we identified SMFRs from 1998 to 2016, using 64-sec-averaged magnetic field and solar wind data obtained from ACE. SMFR identification relies on a determination of the magnetic flux rope structure using model fitting. Many studies have analyzed the geometry of MCs (Farrugia et al. 1993; Marubashi 1997; Shimazu & Vandas 2002; Marubashi & Lepping 2007; Romashets & Vandas 2003). Often, the model scheme for describing the magnetic field structure of an MC is a cylindrical model based on the constant-α force-free concept (Goldstein 1983;

Burlaga 1988). It is characterized by the absence of gravity and plasma pressure, which causes the structure to reside in equilibrium. Its magnetic field can be expressed as

$$B_r = 0 \tag{1}$$

$$B_\phi = HB_0J_1(\alpha r) \tag{2}$$

$$B_z = B_0J_0(\alpha r) \tag{3}$$

where B_0 is the magnetic field strength on a cylindrical axis, $H(= \pm 1)$ is the handedness of the flux rope, r is the radius of the cylinder, and J_n is the nth-order Bessel function. Among the different configuration models of MC, we employed a constant-α, force-free, and self-similar expansion cylinder model (Shimazu & Vandas 2002; Marubashi & Lepping 2007) for SMFR identification. We selected SMFRs through the following steps.

① The candidate SMFR intervals were first selected by requiring that the rotation angle of the magnetic field is greater than 50° in the geocentric solar ecliptic (GSE) Y-Z plane.

② Then, we checked the existence of the typical features of MFRs for the candidate SMFR intervals. The required MFR features include a bipolar signature and enhanced field strength during the duration of the candidate SMFR events.

③ Next, we applied a cylindrical model fitting scheme (Shimazu & Vandas 2002; Marubashi & Lepping 2007) and determined a list of SMFR intervals by requiring that the root mean square (RMS) error of the fitting is less than 0.3.

④ Finally, we improved the accuracy of the boundaries of the determined SMFR intervals by estimating the relative error. Specifically, we removed the events for which the relative error of the boundaries is greater than 0.1.

As a result, we identified a total of 309 SMFR events from 1998 to 2016. To distinguish SMFRs from MCs, we limited the time duration of flux ropes that satisfy the above fitting steps to 12 hr. This is rather arbitrary, but to the authors' knowledge, there is no unique way to define the specific duration with which one can distinguish between SMFRs and MCs.

Fig. 1 shows an example of an SMFR observed on April 23, 1999, which was selected based on the criteria above. The SMFR boundaries are indicated by two black vertical lines and the cylindrical model fit results are shown by the black dot-dashed lines in the first four panels. The duration time
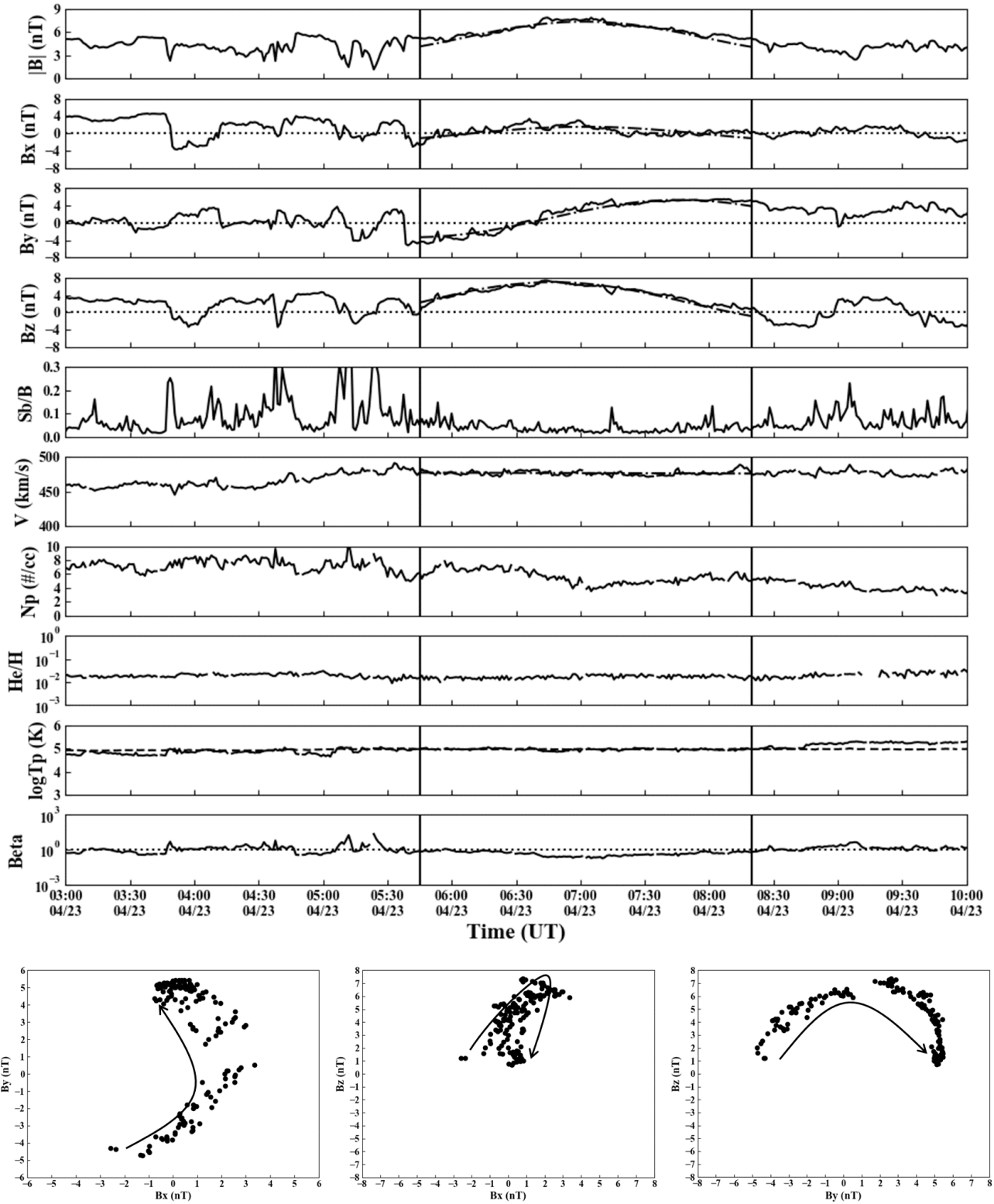
Fig. 1. An SMFR event on April 23, 1999 from ACE. (From top to bottom) The magnetic field intensity, X, Y, and Z components of the magnetic field in the GSE coordinates, the ratio of the standard deviation to the average magnetic field intensity, the solar wind speed, the proton density, the density ratio of He^{++}/H^+, the proton temperature, the plasma beta, and the magnetic field rotations in the X-Y, X-Z, and Y-Z planes during the SMFR interval. The dashed curve along the proton temperature represents the expected temperature from the solar wind speed (Lopez 1987).

Table 1. Number of SMFR events corresponding to the B_z variation type

Type	Number of Events
N	46
NS	107
SN	87
S	69
Total	309

Table 2. Statistical results of SMFRs and MCs

SMFR	$\|B\|$ (nT)	Vsw (km/s)	Np (cc^{-1})	Duration (hr)	Vexp (km/s)
Average	7.4	430.6	7.7	2.5	2.6
Median	6.4	410.1	6.0	1.8	1.9
Standard deviation	4.4	83.0	5.9	2.0	9.4
MC	$\|B\|$ (nT)	Vsw (km/s)	Np (cc^{-1})	Duration (hr)	Vexp (km/s)
Average	10.6	449.0	7.3	26.6	22.0
Median	9.7	428.6	6.4	25.0	18.8
Standard deviation	4.7	95.8	4.2	14.7	40.6

for this SMFR is 155 min, and the maximum field strength is about 8 nT. The B_z of this SMFR is constantly northward and B_y changes from dawn to duskward. The solar wind speed is constant at about 475 km/s. The flat profile of the solar wind speed is a unique feature, in contrast to the MC whose solar wind speed usually decreases during its duration (e.g., Klein & Burlaga 1982). There is practically no difference between the proton temperature and the expected temperature.

We also categorized the identified SMFR events into four types, according to the change in B_z during each SMFR interval. N (S) type refers to an SMFR in which B_z is northward (southward) continuously during the SMFR intervals. In contrast, when B_z changes from northward (southward) to southward (northward) during the intervals, the classification of NS (SN) type is applied. Table 1 shows the results of this classification. NS type has the largest population and N type has the least frequent occurrence.

To compare between the SMFR and MC events, we obtained MC events from the ICME list of Richardson and Cane (Cane & Richardson 2003; Richardson & Cane 2010), available at http://www.srl.caltech.edu/ACE/ASC/DATA/level3/icmetable2.htm. The Richardson and Cane ICME list includes a total of 490 ICME events from 1996 to 2016, with 341 MC events. The results of the comparison are presented in the following section.

3. STATISTICAL PROPERTIES OF SMFR EVENTS

Table 2 shows a summary of the statistical results of SMFRs and MCs, and more specific comparisons are shown in Figs. 2-6. From Table 2, we see that the main difference between SMFRs and MCs occurs in the magnetic field
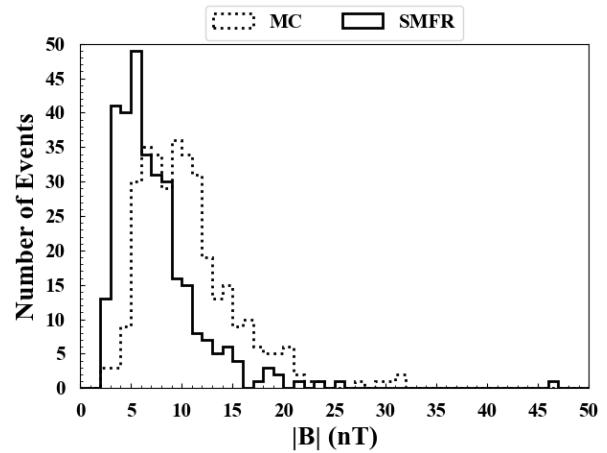
Fig. 2. Distribution of average field strength of SMFRs and MCs.
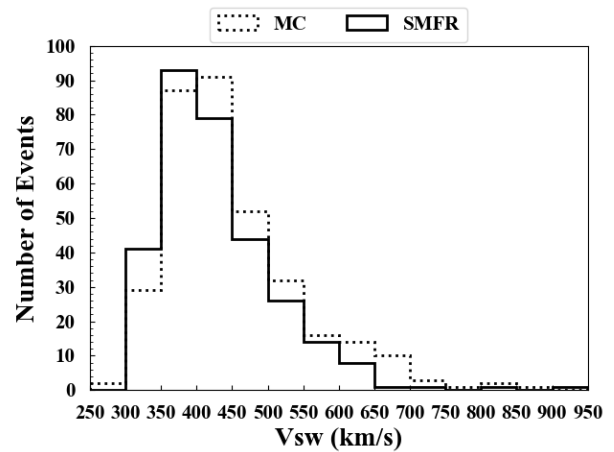
Fig. 3. Distribution for average solar wind speed of SMFRs and MCs.
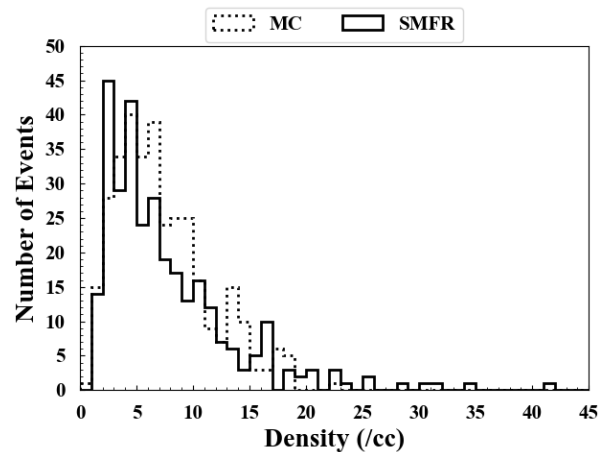
Fig. 4. Distribution of average proton density of SMFRs and MCs.

intensity, duration time, and the expansion speed. The average field strength of the individual SMFRs is 7.4 nT while that of the MCs is 10.6 nT. As for the duration time, the average duration of SMFRs (2.5 hr) is much shorter than
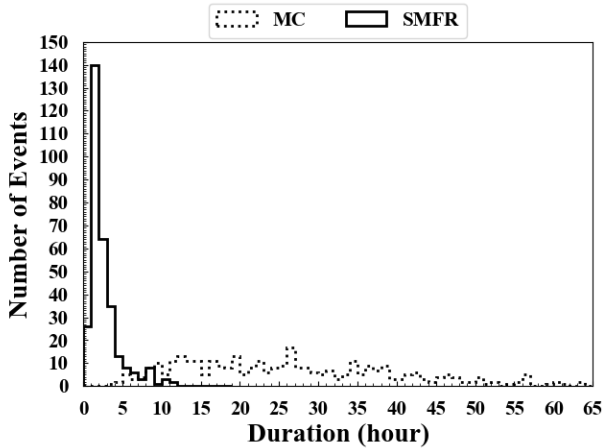
Fig. 5. Distribution for durations of SMFRs and MCs.
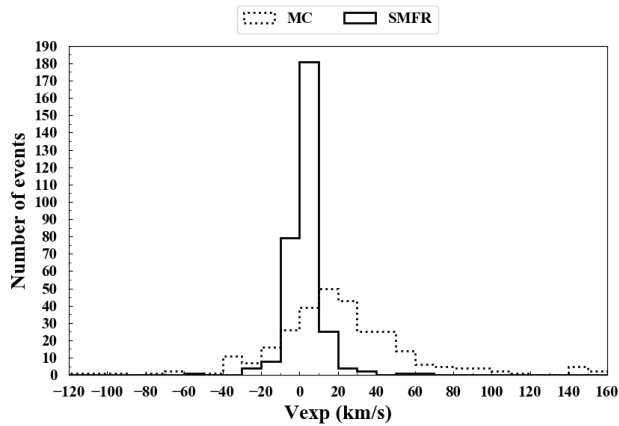
Fig. 6. The distribution of the expansion speed of SMFRs and MCs.

that that of the MCs (26.6 hr). In addition, the average value of the expansion speed for the SMFRs is 2.6 km/s, while that of the MCs is 22.0 km/s.

Fig. 2 shows the distribution of the magnetic field strength of SMFRs and MCs. Regarding MCs, the average field strength varies from 2 nT to 32 nT with two major peaks, one at ~6–7 nT and the other at ~9–10 nT. In contrast, the average field strength of each SMFR varies from 2 nT to 47 nT, with a more pronounced peak at 5 nT.

The solar wind speed distributions of SMFRs and MCs are shown in Fig. 3. The two distributions are very similar and range mostly from 300 km/s to 550 km/s. The average speed of SMFRs is 430.6 km/s, which is only slightly slower than the MC average speed, 449.0 km/s.

Fig. 4 shows the distribution of the average densities of SMFRs and MCs. The density of MCs ranges from 0 to 23 cm^{-3} with a mean value of 7.3 cm^{-3} and a median value of 6.4 cm^{-3}. SMFRs vary over a broader range from 1 cm^{-3} to 42 cm^{-3}, but the distribution of SMFRs is more heavily placed toward a lower density than that of MCs, such that while a

mean value of 7.7 cm^{-3} is slightly larger than that of MCs, the median value of SMFRs is slightly smaller than that of MCs.

Fig. 5 presents the duration times of individual SMFRs and MCs. For 90 % of the SMFR events, the duration is less than 5 hr, and the distribution is strongly peaked at 1–2 hr. In contrast, the duration of MCs is longer than that of SMFRs, extending up to 64 hr. This implies that an SMFR is most likely much smaller than an MC on a spatial scale.

The expansion speed distribution of SMFRs and MCs is presented in Fig. 6. The expansion speed is calculated using the following definition,

$$V_{exp} = \frac{V_{start} - V_{end}}{2} \qquad (4)$$

Most of the SMFR events exhibit velocities between -20 km/s and 20 km/s, with a mean value of 2.6 km/s, while the average expansion speed for MCs is 22.0 km/s, reaching as high as 160 km/s. The results imply that the expansion of SMFR has different characteristics from that of MCs. The solar wind speed profiles of SMFRs as observed near the Earth are nearly flat, as they lack significant expansion while they propagate and are in balance with the ambient solar wind. Unlike SMFRs, MCs do expand during propagation near the Earth, which suggests that they are not in equilibrium with the background solar wind.

4. GEOEFFECTIVENESS OF SMFRS

We examined a possible association of the identified SMFRs with storms and substorms. For this purpose, we checked Sym-H and AL indices during each SMFR event.

Fig. 7 shows an example of the SMFR events observed at ACE on March 20, 2010. The vertical lines in the figure indicate the boundaries of the SMFR event, and the dot-dashed lines in the first four panels show the results of the cylindrical model fitting. B_z changes from southward to northward during the SMFR interval, while B_y is mostly duskward, with the field intensity increasing to about 8 nT. At ~07:00 UT, which we think corresponds to the arrival time of the SMFR, the AL index starts to decrease to about -400 nT, but the SYM-H index remains stable during the SMFR interval. This example demonstrates the possible triggering of substorms, but no storm, by the impact of SMFRs.

We determined the extent to which SMFRs are related to storms and substorms. First, a set of criteria for the SYM-H and AL indices was set to define the occurrence of storms and substorms. For storms, we require that the minimum SYM-H is lower than –50 nT during the SMFR interval. For substorm occurrence, we require that the minimum AL is
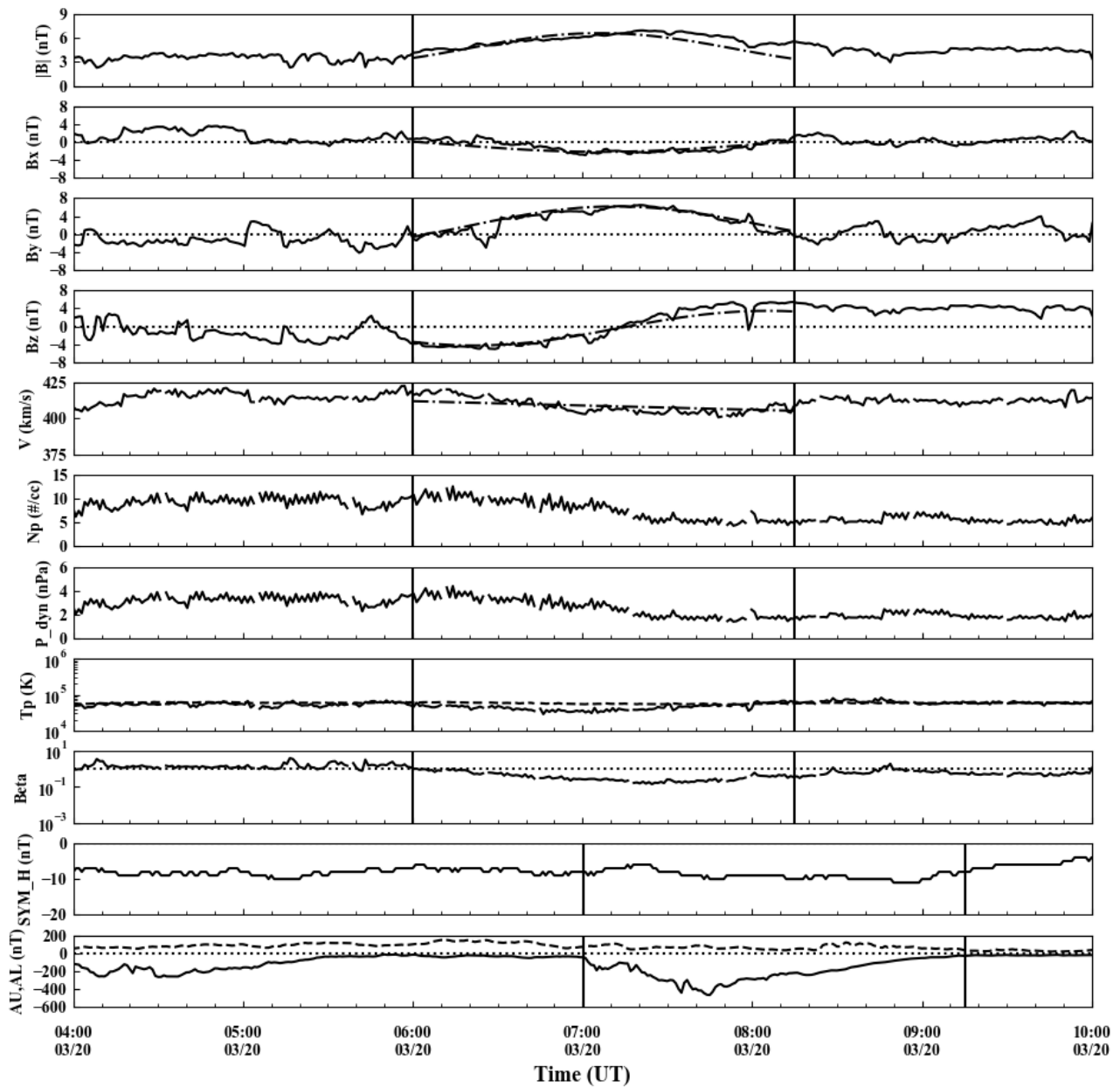
Fig. 7. SMFR event on March 20, 2010 from ACE. The components of the figure from top to bottom are the magnetic field intensity, X, Y, and Z components of the field in the GSE coordinate, solar wind speed, proton density, dynamic pressure, proton temperature, plasma beta, SYM-H, and the AU and AL indices. The dashed curve along the proton temperature represents the expected temperature from the solar wind speed. The solar wind data here has not been time-shifted.

lower than -200 nT during the SMFR interval. Table 3 shows the statistics on the association between SMFRs and storms/substorms. They indicate that 23 (7.4 %) of the total SMFRs are storm-related, while 161 (52.1 %) meet the substorm criteria. The percentage of association with substorms for each type of SMFR is highest for S type SMFRs (66.7 %), followed by SN type (64.4 %), NS type (46.7 %), and N type (19.6 %).

In obtaining the results in Table 3, the association was

identified as long as Sym-H and AL met the threshold values anytime during the SMFR intervals. To determine the causality relationship between SMFR and storms/substorms more precisely, namely, for an SMFR to be considered as an actual trigger of a storm/substorm, we imposed a more rigorous criterion. Specifically, the decrease of Sym-H (less than -50 nT) and AL (less than -200 nT) should be preceded by a period of quiet state before the arrival of SMFR events. In other words, only events where Sym-H and AL began to

Table 3. Statistics of the SMFR events associated with storms and substorms

B_z type	Number of events	
	Storm	Substorm
N	1 (2.2%)	9 (19.6%)
NS	10 (9.3%)	50 (46.7%)
SN	5 (5.7%)	56 (64.4%)
S	7 (10.1%)	46 (66.7%)
Total	23 (7.4%)	161 (52.1%)

Table 4. SMFR statistics associated with storms and substorms based on a more rigorous criterion

B_z type	Number of events	
	Storm	Substorm
N	0	2 (4.3%)
NS	2 (1.9%)	35 (32.7%)
SN	0	25 (28.7%)
S	0	26 (37.7%)
Total	2 (0.6%)	88 (28.5%)

decrease after the arrival of SMFR events were considered. In this sense, we regard such storm and substorm events as indeed triggered by SMFR impact. A classification from this more stringent criterion is presented in Table 4. Not surprisingly, the percentage of association between SMFRs and substorms/storms decreases. Specifically, the number of storms triggered by SMFRs is 2 (0.6 %), implying that SMFRs rarely trigger storms, which is not surprising at all considering the intrinsic property of the small magnetic field intensity of the SMFR. In contrast, 88 (28.5 %) of the total SMFRs trigger substorms. The interesting aspect is that 70 % of substorms are due to the NS and SN types that involve a change in the B_z direction.

5. SUMMARY AND CONCLUSIONS

In this study, we identified a total of 309 SMFRs from 1998 to 2016 using ACE data. The identified SMFRs have different magnetic field strengths, expansion speeds, and duration times than MCs. The mean value of the field strength of MCs and SMFRs are 10.6 nT and 7.4 nT, respectively, implying that SMFR has a weaker magnetic flux rope structure. The duration times of MCs and SMFRs are 26.6 hr and 2.5 hr, respectively, which means that the size of SMFRs is much smaller than that of MCs. In particular, the difference in the expansion speed (22.0 km/s for MCs vs. 2.6 km/s for SMFRs) indicates that the condition of the two groups near the Earth is different. MCs were expanding when observed by ACE. In contrast, most of SMFRs must have finished expansion when they were observed near the Earth, regardless of their origin, whether originated from solar eruptions or not.

We also examined the geoeffectiveness of SMFRs, based on a set of criteria regarding decreases in Sym-H and AL to define the occurrence of storms and substorms. We found that 53 % of all SMFRs appear to be related to substorms, but use of a more rigorous criterion indicates that ~28.5 % of SMFRs may have actually triggered substorms. In contrast, the association percentage with storms is negligible. This result means that the conditions of SMFRs are insufficient to cause a storm, but they can often trigger a substorm. While

this is not a new finding, our results confirm it using a larger database than in previous studies.

In conclusion, SMFRs studied here are magnetic flux ropes that are of a much smaller spatial scale, a weaker magnetic field strength, and less expansion near the Earth, as compared to the normal magnetic flux ropes of normal MCs. The geoeffectiveness of SMFRs may be substantial from the viewpoint of (or at least association with) substorm triggering. We emphasize that all these findings are not entirely new; rather they have been corroborated based on a much larger database than in previous studies. We suggest the possibility that this smaller scale flux rope structure may exist at a much higher occurrence rate than normal magnetic clouds that are ejected mostly when the Sun is active (Hwangbo et al. 2015; Lee 2015). A further study is desired to determine the solid occurrence rate of SMFRs as compared to that of larger MC events. Ultimately, the origin of SMFRs remains a fundamental question that warrants future research.

ACKNOWLEDGMENTS

REFERENCES

Burlaga LF, Magnetic clouds and force-free fields with constant alpha, J. Geophys. Res. 93, 7217–7224 (1988). https://doi.org/10.1029/JA093iA07p07217

Cane HV, Richardson IG, Interplanetary coronal mass ejections in the near-Earth solar wind during 1996–2002, J. Geophys. Res. 108, 1156 (2003). https://doi.org/10.1029/2002JA009817

Cartwright ML, Moldwin MB, Comparison of small-scale flux rope magnetic properties to large-scale magnetic clouds: Evidence for reconnection across the HCS? J. Geophys. Res. 113, A09105 (2008). https://doi.org/10.1029/2008JA013389

Cartwright ML, Moldwin MB, Heliospheric evolution of solar wind small-scale magnetic flux ropes, J. Geophys. Res. 115, A08102 (2010). https://doi.org/10.1029/2009JA014271

Farrugia CJ, Burlaga LF, Osherovich VA, Richardson IG, Freeman MP, et al., A study of an expanding interplanetary magnetic cloud and its interaction with the Earth's magnetosphere: The interplanetary aspect, J. Geophys. Res. 98, 7621–7632 (1993). https://doi.org/10.1029/92JA02349

Feng HQ, Wu DJ, Lin CC, Chao JK, Lee LC, et al., Interplanetary small- and intermediate-sized magnetic flux ropes during 1995–2005, J. Geophys. Res. 113, A12105 (2008). https://doi.org/10.1029/2008JA013103

Goldstein H, On the field configuration in magnetic clouds, in Solar Wind Five, eds. M. Neugebauer (NASA, Washington D.C., 1983), 731–733.

Gosling JT, Pizzo V, Bame SJ, Anomalously low proton temperatures in the solar wind following interplanetary shock waves—evidence for magnetic bottles?, J. Geophys. Res. 78, 2001–2009 (1973). https://doi.org/10.1029/JA078i013p02001

Gosling JT, McComas DJ, Phillips JL, Bame SJ, Geomagnetic activity associated with earth passage of interplanetary shock disturbances and coronal mass ejections, J. Geophys. Res. 96, 7831–7839 (1991). https://doi.org/10.1029/91JA00316

Gopalswamy N, Yashiro S, Xie H, Akiyama S, Mäkelä P, Properties and geoeffectiveness of magnetic clouds during solar cycles 23 and 24, J. Geophys. Res. 120, 9221–9245 (2015). https://doi.org/10.1002/2015JA021446

Hwangbo JE, Bong SC, Park SH, Lee DY, Cho KS, et al., Burst locating capability of the Korean solar radio burst locator (KSRBL), J. Astron. Space Sci. 32, 91-99 (2015). https://doi.org/10.5140/JASS.2015.32.1.91

Klein LW, Burlaga LF, Interplanetary magnetic clouds At 1 AU, J. Geophys. Res. 87, 613–624 (1982). https://doi.org/10.1029/JA087iA02p00613

Lee J, Recent progress in understanding solar magnetic reconnection, J. Astron. Space Sci. 32, 101-112 (2015). https://doi.org/10.2140/JASS.2015.32.2.101

Lopez RE, Solar cycle invariance in solar wind proton temperature relationships, J. Geophys. Res. 92, 11189–11194 (1987). https://doi.org/10.1029/JA092iA10p11189

Marubashi K, Interplanetary Magnetic Flux Ropes and Solar Filaments, in Coronal Mass Ejections, vol. 99, Geophysical Monohraph Series, eds. Crooker N, Joselyn JA, Feynman J (American Geophysical Union, Washington, D.C. 1997) 147-156.

Marubashi K, Lepping RP, Long-duration magnetic clouds: a comparison of analyses using torus- and cylinder-shaped flux rope models, Ann. Geophys. 25, 2453-2477 (2007). https://doi.org/10.5194/angeo-25-2453-2007

Moldwin MB, Phillps JL, Gosling JT, Scime EE, McComas DJ, et al., Ulysses observation of a noncoronal mass ejection flux rope: Evidence of interplanetary magnetic reconnection, J. Geophys. Res. 100, 19903–19910 (1995). https://doi.org/10.1029/95JA01123

Moldwin MB, Ford S, Lepping R, Slavin J, Szabo A, Small-scale magnetic flux ropes in the solar wind, Geophys. Res. Lett. 27, 57–60 (2000). https://doi.org/10.1029/1999GL010724

Park W, Lee J, Yi Y, Ssessanga N, Oh S, Storm sudden commencements without interplanetary shocks, J. Astron. Space Sci. 32, 181-187 (2015). https://doi.org/10.5140/JASS.2015.32.3.181

Romashets EP, Vandas M, Force-free field inside a toroidal magnetic cloud, Geophys. Res. Lett. 30, 2065 (2003). https://doi.org/10.1029/2003GL017692

Richardson IG, Cane HV, Regions of abnormally low proton temperature in the solar wind (1965–1991) and their association with ejecta, J. Geophys. Res. 100, 23397–23412 (1995). https://doi.org/10.1029/95JA02684

Richardson IG, Cane HV, Near-Earth interplanetary coronal mass ejections during solar cycle 23 (1996–2009), Sol. Phys. 264, 189-237 (2010). https://doi.org/10.1007/s11207-010-9568-6

Shimazu H, Vandas M, A self-similar solution of expanding cylindrical flux ropes for any polytropic index values, Earth Planets Space 54, 783–790 (2002). http://doi.org/10.1186/BF03351731

Tsurutani BT, Gonzalez WD, The Interplanetary Causes of Magnetic Storms: A Review, in Magnetic Storm, vol. 98, Geophysical Monograph Series, eds. Tsurutani BT, Gonzalez WD, Kamide Y, Arballo JK (American Geophysical Union, Washington, D. C. 1997), 77-89.

Wu CC, Liou K, Lepping RP, Hutting L, Plunkett S, et al., The first super geomagnetic storm of solar cycle 24: the St. Patrick's day event (17 March 2015). Earth Planets Space 68, 151 (2016). https://doi.org/10.1186/s40623-016-0525-y

Zhang G, Burlaga LF, Magnetic clouds, geomagnetic disturbances, and cosmic ray decreases, J. Geophys. Res. 93, 2511–2518 (1988). http://doi.org/10.1029/JA093iA04p02511

Zhang J, Richardson IG, Webb DF, Gopalswamy N, Huttunen E, et al., Solar and interplanetary sources of major geomagnetic storms (Dst ≤ −100 nT) during 1996–2005, J. Geophys. Res. 112, A10102 (2007). https://doi.org/10.1029/2007JA012321